Research Article | Vol. 28, No. 25 / 7 December 2020 / Optics Express 38206
Optics EXPRESS

Performance analysis of a silicon NOEMS device applied as an optical modulator based on a slot waveguide

YU FENG,[1,3] DAVID J. THOMSON,[2] GORAN Z. MASHANOVICH,[2] AND JIZE YAN[1,4]

[1]Electronics and Computer Science, University of Southampton, Southampton SO17 1BJ, UK
[2]Optoelectronics Research Centre, University of Southampton, Southampton SO171BJ, UK
[3]yf1g15@soton.ac.uk
[4]j.yan@soton.ac.uk

Abstract: In this paper, we analyse the performance of a silicon nano-opto-electro-mechanical system (NOEMS) applied as an optical modulator, based on a suspended slot waveguide driven by electrostatic forces. The analysis is carried out with the help of the finite element analysis (FEA) method involving the influences from Casimir force, optical force and electrostatic force. The performance of the modulator are analysed from aspects of actuating modes, actuating voltage, modulating frequency, effective index, phase change, and energy consumption using the FEA method. Simulation results show that a suspended slot modulator has the advantages of low actuation voltage, low power consumption, as well as large effective index and phase change compared with modulators based upon other approaches. The performance of such a modulator can fill the performance gap between the carrier-based approach and micro-opto-electro-mechanical system (MOEMS) approach for modulation.

1. Introduction

Slot waveguides are constructed of a slot of low index material sandwiched between slots with arms of high-index material. The high-index-contrast interfaces on the boundaries of the slot produce large discontinuities in the electric field with a much higher amplitude in the low-index side [1]. Thus, the optical field can be enhanced and confined in the low-index region when light is guided by total internal reflection [1]. The differing amounts of field enhancement on the inner or outer boundary surfaces of the slot arms contribute to attractive/repulsive optical forces on the slot waveguides [2,3]. Apart from optical force, Casimir force on the inner boundary surfaces can not be ignored in some cases. Casimir force is a dispersive force originating from a fluctuating electromagnetic field within the two dissipative media [4]. This is the dominant interaction between uncharged materials within a nanometer-scale range and is strong enough to cause collapsing and adhesion between movable parts.

For a silicon platform, the slot waveguide can be constructed on silicon-on-insulator (SOI) where silicon and the surrounding air are treated as the high-index and low-index materials respectively. In this case, the optical field is mainly confined and enhanced in the air cladding as an evanescent field. Based on the fact that the optical mode of the waveguide can be modified by altering the separation of the slot arms, slot waveguides on SOI can form a Nano-Opto-Electro-Mechanical System (NOEMS) device capable of all-optical [5] and electro-optical [6] control by suspending the waveguides through removal of the underlaying silicon oxide. Beyond the controllable optical force and electrostatic force, Casimir force can be helpful with actuation while it also sets limitations on the performance of the device [7,8].

#411933 https://doi.org/10.1364/OE.411933
Journal © 2020 Received 8 Oct 2020; revised 29 Oct 2020; accepted 1 Nov 2020; published 2 Dec 2020

Optics EXPRESS

Phase modulation is one of the key functionalities in a silicon photonics circuit. Modulation can be carried out using the thermo-optic effect, plasma dispersion effect and MOEMS approaches [9]. The thermo-optical and MOEMS approaches are slow and relatively power hungry, whereas the plasma dispersion approach is fast (over Gb/s) but results in relatively large optical losses and a weak modulation effect [6]. The suspended slot modulator is regarded as one of the NOEMS approaches to improve on the performance from MOEMS devices. Currently, there are few publications about optical modulators based upon the suspended slot waveguide approach. The understanding about the performance of such a device is insufficient, though some measurements are taken in [6] and [10] to quantify the modulator performance based on specific designs and some analysis about system limitations are investigated by [7,8]. As a device making use of electro-refraction [11] from optomechanical deformation, the features of the suspended slot modulator are not clearly investigated yet. In this paper, we describe a theoretical performance analysis of a slot-based NOEMS applied as an electro-optical modulator from the aspect of working modes, actuating voltage, modulating frequency, effective index, phase change, and energy consumption (J/bit). To investigate the features of the modulator, suspended slots with different suspension lengths are investigated involving the known physical models including Optical force, electrostatic force, and Casimir force.

The design of the device and related theoretical analysis including optical force, electrostatic force, Casimir force, operating mode and states, pull-in effect, modulating frequency, and opto-mechanical refractive index and phase change are illustrated in section 2. Calculation results and discussion about the system in the pulse and resonant modes at the 'one' and 'zero' states of the device corresponding to section 2 are described in section 3 Conclusions and summarising are in section 4.

2. Design and theoretical analysis

In this section, we propose a model for suspended slot waveguides on SOI applied as a nano-opto-mechanical modulator. The basic idea of the modulator is achieved by replacing part of the regular waveguide with a suspended slot waveguide so that effective index and phase can be manipulated with a nano-opto-mechanical actuator. The opto-mechanically induced index change, phase change, and its operating frequency are key parameters in the modulator design. The physical phenomenon in suspended slot waveguides include opto-mechanical deformation, optical force and Casimir force [7,8]. Electrostatic force used as the source of actuation is analysed as well. The photoelastic effect of the deformable waveguide is negligible [12]. The waveguide configuration and field distribution of the fundamental quasi-TE mode is shown in Fig. 1.

2.1. Casimir force

From Lifshitz theory, the Casimir force (F_{Cas}) between two real material plates, separated by a gap distance g, is expressed by adding a correction factor to the Casimir force for ideal conductor plates, which leads to [4]

$$F_{cas}(g, A) = -\frac{\hbar c \pi^2}{240} \frac{A}{g^4} \eta \tag{1}$$

where $\hbar$ is the reduced Planck constant, A is the area of the plates, and η is the nite conductivity correction factor, which depends on the dielectric permittivities of the material in the system. The influence of the temperature T is usually negligible for a NOEMS, since photon energy dominates the system rather than phonon energy ($g \ll c\hbar/k_B T$), where k_B is the Boltzmann

Optics EXPRESS

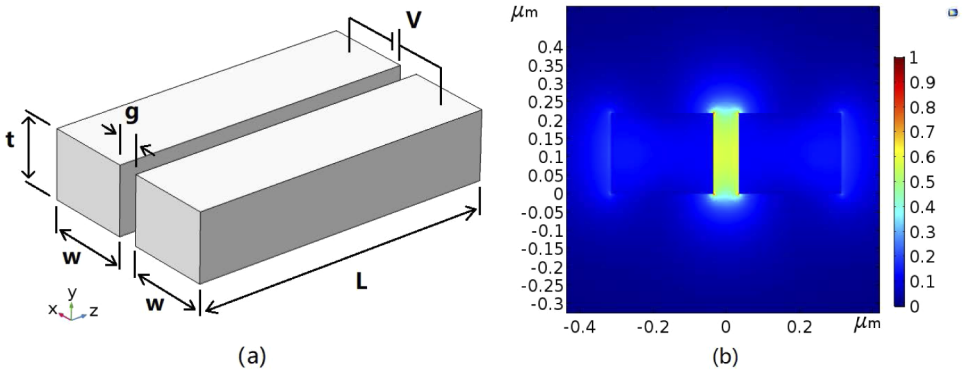

Fig. 1. (a) Configuration of suspended slot waveguide; (b) Fundamental Quasi-TE mode of the waveguide from COMSOL Multiphysics, color bar indicates normalised electric field intensity

constant [4]. For identical dielectric parallel plates:

$$\eta = \left(\frac{\epsilon - 1}{\epsilon + 1}\right)^2 \left(1 - \frac{1.11}{\sqrt{\epsilon}} \ln \frac{\epsilon}{7.6}\right) \tag{2}$$

where ϵ is the dielectric permittivity of the material. For silicon with refractive index equal to 3.475, with approximation of $n = \sqrt{\epsilon}$, the correction factor is calculated to be $\eta \approx 0.611$.

2.2. Optical force

The optical force on the slot waveguide is attractive for a symmetric mode, while the force will be repulsive for an asymmetric mode [13]. By neglecting the opto-elastic effect inside the silicon [14], the optical force for monochromatic light in a slot waveguides can be calculated by [2,13]

$$F_{opt} = -\frac{L}{c} \frac{dn_{eff}}{dg}\bigg|_{\omega} P_{opt} \tag{3}$$

where n_{eff} , L, P, and ω represent the effective refractive index, length of the waveguide, optical power, and frequency, respectively. The mechanical load induced by both kinds of force is uniformly distributed along the waveguide from an initial static equilibrium with a constant g.

2.3. Electrostatic force

For electrostatic actuation, the force can be derived by differentiating the electrical potential energy ($P.E.$) stored in the capacitive structure given by

$$F_{es} = \frac{dP.E.}{dx} \tag{4}$$

$$P.E. = \frac{CV^2}{2} \tag{5}$$

$$C = \frac{\epsilon A}{g} \tag{6}$$

where C is the capacitance of the structure and V is the potential applied on the structure. A and g represent overlap area and gap (distance between two plates) of the capacitor. Thus the

Optics EXPRESS

electrostatic force with DC voltage applied on a parallel-plate capacitor is

$$F_{es} = \frac{dP.E.}{dg} = \frac{1}{2}V^2\frac{\partial C}{\partial g} \tag{7}$$

Using electrostatic actuation, a voltage difference must be applied between the moveable structure and its target deflection direction. For the case of a slot waveguide, the parallel plate cannot be treated as an ideal capacitor as Eq. (6) due to its low t/w ratio. The capacitance of the slot waveguide needs to be solved numerically. For the suspended slot modulator in this paper, the mechanical structure can be actuated by not only a pulse wave but also a sinusoidal wave. A general expression for the actuation voltage containing DC and AC terms is described by:

$$V = V_{DC} + |V_{AC}|\cos(\omega t) \tag{8}$$

By substituting Eq. (8) into Eq. (7), the full expression for electrostatic force is described by:

$$F_{es} = -\frac{1}{2}\left\{{V_{DC}}^2 + \frac{|V_{AC}|^2}{2} + 2V_{DC}|V_{AC}|\cos\omega t + \frac{|V_{AC}|^2}{2}\cos 2\omega t\right\}\frac{\partial C}{\partial g} \tag{9}$$

2.4. Operating mode and state of the modulator

Generally, the modulator can be operated with different wave forms in a frequency range that system is able to respond to. Square wave and sinusoidal wave are typical wave forms in digital and analogue electrical and electronic devices. For the dedicated modulator in this paper, modulation with square wave is described as pulse mode of the modulation covering frequency ranging from 0 to f_{max}^{pulse} estimated by Eq. (25). Modulation with sinusoidal wave is described as sinusoidal mode of modulation covering frequency ranging from 0 to ω_{res} estimated by Eq. (27). The best performance in the sinusoidal mode can be obtained when the modulator is operated around the mechanical resonant frequency due to significant mechanical amplitude amplification as described in Eq. (28). This specific case is described as resonant mode in this paper.

During the modulation, every bit of data is represented by a high (one) or a low (zero) energy level corresponding to the maximum index state or minimum index state of the waveguide, respectively, or reversely. If we assume every one and zero correspond to the maximum index state and minimum index state of the waveguide, respectively, mechanical deformation curvatures at the one and zero states in the pulse and sinusoidal mode are as shown in Fig. 2. As can be seen in Fig. 2, in the pulse mode, 'zero' is the state that has no actuating voltage applied on the waveguide (Casimir force and optical force only), while 'one' is the state where the slot is actuated by electrostatic force. In the sinusoidal mode, 'zero' is the state when the two slot arms reach their maximum separation, while 'one' is the state when the separation is at a minimum. In order to simplify the analysis in the pulse and sinusoidal modes, we treat Eq. (9) as Eq. (10) and Eq. (11) described by:

$$F_{es}^{sine} \approx -\frac{1}{2}\left\{\frac{|V_{AC}|^2}{2} + A\frac{|V_{AC}|^2}{2}\cos 2\omega t\right\}\frac{\partial C}{\partial g} \tag{10}$$

$$F_{es}^{pulse} \approx -\frac{1}{2}{V_{DC}}^2\frac{\partial C}{\partial g} \tag{11}$$

where F_{es}^{sine} and F_{es}^{pulse} are the electrostatic forces applied on the device corresponding to the sinusoidal and pulse modes. In Eq. (10), A denotes for amplitude amplification factor. In the pulse mode, V_{AC} is not considered while in the sinusoidal mode, V_{DC} is neglected in the analysis. The DC term in Eq. (10) together with Casimir force and optical force provide a constant bias force that breaks the symmetry of the deformation curvature at the 'zero' and 'one' states to the straight slot in the sinusoidal mode.

Optics EXPRESS

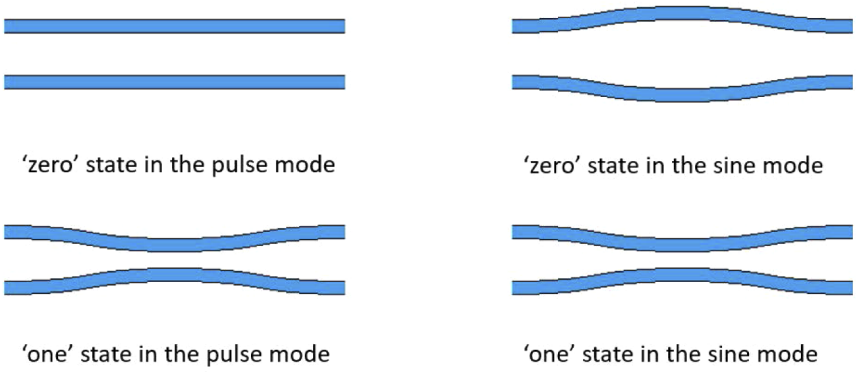

Fig. 2. Top view of 'zero' and 'one' state of modulator in the pulse mode and sinusoidal mode

2.5. Mechanical deformation and pull-in effect

The curvature of the slot arm under a distributed load expressed with the Euler-Bernoulli beam equation is shown by (residual axial stress neglected) [15]:

$$EI\frac{d^4\delta(z)}{dz^4} = p_m(z) \tag{12}$$

where E is Young's modulus, $p_m(z)$ is the load (N/m) distribution along the one dimensional beam and I is the beam's area moment of inertia. In the direction of interest I is solved as $I = tw^3/12$, where w and t are the width and thickness of the beam, respectively. With a uniformly distributed load, the formula for the deflection curvature is described by [16]:

$$\delta(z) = \frac{p_m z^2}{24EI}(L-z)^2 \tag{13}$$

Based on the fact that F_{cas}, F_{opt} and F_{es} on each section of the beam will increase with the decreasing slot arm separation, the load exerted on the centre part of the beam must be larger than the load on the rest part of the beam. So rather than initial equilibrium, deformation of the beam induces the load distribution non-uniformly, which eventually enhances the force by decreasing g as:

$$g(z) = g_0 - 2\delta(z) \tag{14}$$

$p_m(z)$ in this case is expressed as:

$$p_m(z) = \frac{F_{opt}(g(z))}{L} + \frac{F_{es}(g(z))}{L} + \frac{F_{cas}(g(z))}{L} \tag{15}$$

With constant load in an elastic range, the structure has enough restoring force to balance the external load, thus the system will reach a steady state or quasi-static state. However, due to the enhanced electromagnetic load with beam separation decreasing according to Eq. (1), Eq. (3) and Eq. (7), load redistribution happens with beam deformation further enhancing the electromagnetic load and Casimir load, which forms a positive feedback. Thus the equilibrium of the restoring force and electromagnetic load can not be maintained for long before material failure. This is referred to pull-in effect [17] and it sets a critical value (energy limitation) of the system failure. For electrostatic actuation, the maximum voltage allowed for actuation is referred

Optics EXPRESS

to as the pull-in voltage V_{PI} expressed by [18]:

$$V_{PI} = \sqrt{\frac{8}{27}\frac{{g_0}^2 K}{\epsilon A}} \tag{16}$$

where K is the mechanical effective stiffness when the structure is applied with the pull-in voltage. This is a theoretical approximation by treating the movable part and its actuator as a linear spring-mass model and an ideal parallel-plate capacitor, respectively. The accurate value of the pull-in voltage needs to be solved numerically. In the later analysis, the suspended slot in the pull-in state is regarded as the 'one' state of the modulator.

2.6. Opto-machanical refractive index and phase change

Due to the deflection curvature, the effective refractive index distribution along the waveguide is not uniform, thus the overall effective refractive index change should be evaluated by integrating the index change along the entire suspended waveguide length. The overall index change can be expressed as:

$$\Delta n_{eff} L = \int_0^L [n_{eff}(g_2(z)) - n_{eff}(g_0)]dz - \int_0^L [n_{eff}(g_1(z)) - n_{eff}(g_0)]dz \tag{17}$$

where $g_1(z)$ and $g_2(z)$ is the arm separation in the 'zero' state of the modulation, and the 'one' state of the modulation, respectively. An analytical approximation of the index change can be made by combining the deformation curvature by Eq. (13) and equivalent load (p_e) at the maximum deformation (δ_{max}) in the middle point ($z = L/2$) of the curvature calculated by quasi-static analysis in FEA software, expressed by:

$$\delta^e_{max} = \frac{p_e L^4}{384EI} \tag{18}$$

Treating the $\Delta n_{eff}/\Delta g$ as a factor D in the case of small deformation, the overall index change approximation can be expressed as:

$$\Delta n_{eff} L = (p_{e2} D_2 - p_{e1} D_1)\frac{L^5}{360EI} \tag{19}$$

where p_{e1}, p_{e2}, D_1, D_2 denote the 'zero'/'one' state equivalent loads and 'zero'/'one' state effective index change rates, respectively. It can be further simplified by maximum deformation ($\delta^{e1}_{max}, \delta^{e2}_{max}$) expression as:

$$\Delta n_{eff} L = (\delta^{e2}_{max} D_2 - \delta^{e1}_{max} D_1)\frac{49}{45}L \tag{20}$$

The phase change of the light in the waveguide responds to index change is expressed as:

$$\Delta\phi = \Delta n_{eff} L\frac{2\pi}{\lambda} = (\delta^{e2}_{max} D_2 - \delta^{e1}_{max} D_1)\frac{49}{45}L\frac{2\pi}{\lambda} \tag{21}$$

This approximation can be used to evaluate the load distribution by comparing the approximated value with FEA results.

2.7. Modulating frequency

From a typical lump model of the single-degree-of-freedom (SDOF) mechanical resonator including mass M, spring K and damper C, the time constant τ of a step input signal can be

Optics EXPRESS

expressed as:

$$\tau = \frac{1}{\omega_n \zeta} = \frac{2Q}{\omega_n} = \frac{2M}{C} \tag{22}$$

$$\omega_n = \sqrt{\frac{K}{M}} \tag{23}$$

where ω_n, ζ and Q denotes natural frequency, damping factor and quality factor, respectively. The main damping mechanisms involved in the system can be classified as thermoelastic damping [19], air damping [20] and support loss [21]. For clamped-clamped beams such as is the case with the suspended slot waveguide, thermoelastic damping and support loss are negligible compared with air damping. The natural frequency and thermoelasitic quality factor can be solved by using COMSOL Multiphysics while air damping for a double clamped beam can be calculated from [20]:

$$\zeta_{air} = \frac{\alpha \mu L^2}{4.73^2 t^2 w} \sqrt{\frac{3}{E\rho}} \tag{24}$$

where α is a constant related to the Reynolds number, and μ is the dynamic viscosity of the air. Following [20], $\alpha = 10$ and $\mu = 1.81 * 10^{-5} Ns/m^2$.

For 2-DoF system, which is exactly the case of the suspended slot modulator, the lump models of identical resonators coupled with a spring (K_c) are as shown in Fig. 3. Two mechanical resonant modes exist in a 2-DoF system. The overall feature of the target mode is identical with a SDOF system with $K = K_0 + 2K_c$. In this paper, the electromagnetic spring contributes to negative stiffness and as a result the resonant frequency will be lower than with a single beam. The time constant of the system does not change since it is stiffness independent.

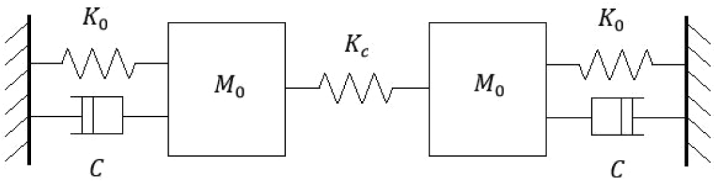

Fig. 3. Lump model for slot modulator, K_0 and M_0 is the mechanical stiffness and mass of one arm of the slot waveguide. K_c is the equivalent stiffness induced by Casimir force, optical force and electrostatic force

When the modulator is working in the pulse mode, the value of maximum modulating frequency depends on its system response time. If the settling time of the system is regarded as 3τ, corresponding to the step input signal (square wave), the maximum modulation frequency with pulse modulation with 50% duty cycle is expressed as:

$$f_{max}^{pulse} = \frac{1}{6\tau} = \frac{\omega_n \zeta}{6} \tag{25}$$

When the modulator is working in the sinusoidal mode, the system is actuated with a sinusoidal signal at frequency ω. Unlike the pulse mode, the periodic actuating force is amplified by factor A expressed as [22]:

$$A = \frac{1}{\sqrt{(1-\gamma^2)^2 + (2\gamma\zeta)^2}} \tag{26}$$

where γ is the ratio between input frequency and natural frequency ω/ω_n.

Optics EXPRESS

When the modulator is working in the resonant mode, the system is operated around the resonant frequency. The mechanical resonant frequency and corresponding force amplification factor are described as:

$$\omega_{res} = \omega_n \sqrt{1 - 2\zeta^2} \tag{27}$$

$$A_{res} = \frac{1}{2\zeta\sqrt{1-\zeta^2}} \tag{28}$$

The amount of actuating force required is A_{res} times less to reach the same deformation curvature as in the pulse mode. Therefore, resonant modulation can achieve a higher operating frequency with less energy consumption (lower voltage) compared with the modulator operating in pulse modulation mode.

To compare the performance between resonant modulation and pulse modulation, we use a pull-in displacement the same as that in the 'one' state of the pulse mode to evaluate the performance in the resonant mode. According to Eq. (10), the actuating voltage at resonance should be described by:

$$\frac{|V_{AC}|^2}{2} + A_{res}\frac{|V_{AC}|^2}{2} = (V_{PI})^2 \tag{29}$$

By solving the equation, the actuating voltage in the resonant mode is described by:

$$|V_{AC}| = V_{PI}\sqrt{\frac{2}{1 + A_{res}}} \tag{30}$$

where $|V_{AC}|$ is always smaller than V_{PI} since A_{res} is always larger than 1 if a resonance exists ($0<\zeta<\frac{\sqrt{2}}{2}$). Then, the electrostatic force in the 'zero' state can be described by:

$$F_{es0}^{sine} \approx -\frac{1}{2}\left\{\frac{|V_{AC}|^2}{2} - A_{res}\frac{|V_{AC}|^2}{2}\right\}\frac{\partial C}{\partial g} = \frac{1 - A_{res}}{1 + A_{res}}F_{es1}^{sine} \tag{31}$$

where F_{es0}^{sine} and F_{es1}^{sine} denote the electrostatic force in the 'zero' and 'one' state, respectively.

3. Results and discussion

To numerically quantify the modulator, COMSOL Multiphysics is used to simulate the structure. The thickness of the silicon layer is chosen to be 220 *nm* which is commercially available and suitable for a wavelength of 1550 *nm*. The width and the gap of the slot waveguide is chosen to be 280 *nm* and 70 *nm*, respectively. The mechanical properties of the silicon are set as those used in [21]. The optical force from the fundamental quasi-TE mode only is analysed in this section. The performance limitations of the design are illustrated for the device in both the pull-in and initial states, covering the upper and lower limits of the modulation performance. The initial state of the modulator is defined as the state when there is no voltage applied to the device with light going through the waveguide (Casimir force and optical force), while the pull-in state involves all forces under consideration. To describe the theoretical best performance of the device, the pull-in state is regarded as the 'one' state and the initial state is regarded as the 'zero' state of the modulator. Casimir force is calculated from Eq. (1) and Eq. (2). Optical force and electrostatic force are calculated using the wave optics module and electrostatic module of COMSOL multiphysics, respectively. The effective refractive index of the fundamental quasi-TE mode with different gap widths are calulated with Lumerical's mode solutions module which is consistent with the results from the wave optics module of COMSOL multiphysics. The calculated effective refractive index results for different gap widths are shown in Fig. 4(a). The load-gap relation of the Casimir force, optical force and electrostatic force are shown in Fig. 4(b). In order to illustrate load-gap relation of the power dependent forces $F_{es}(pN/\mu m/V^2)$ and $F_{opt}(pN/\mu m/W)$ with $F_{cas}(pN/\mu m)$ together

Optics EXPRESS

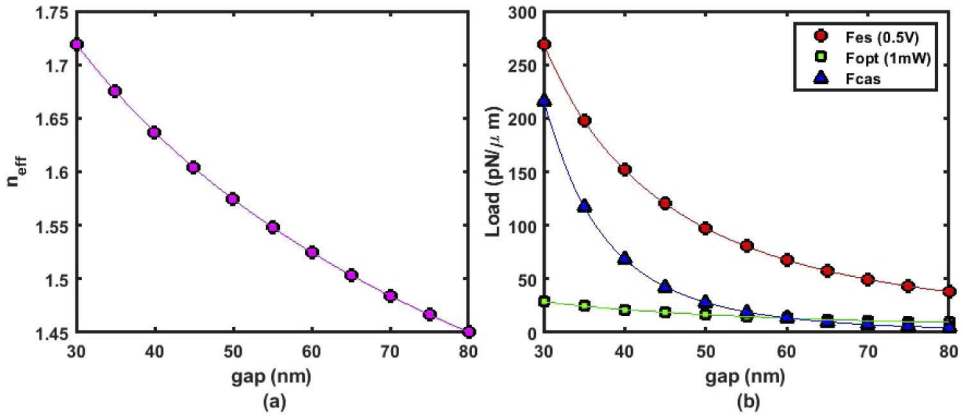

Fig. 4. (a) Effective refractive index (n_{eff}) of quasi-TE mode with different gap widths of the modulator; (b) Load of Electrostatic force (Fes) at 0.5V, Optical force (Fopt) at 1mW, and Casimir force with different gap widths in the modulator.

in Fig. 4(b), F_{es} and F_{opt} are calculated under an input voltage of 0.5 V and input optical power of 1 mW, respectively.

The attractive forces between the two slot arms are equivalent to a nonlinear mechanical connection with negative stiffness. The three types of force analysed in this model have individual force-gap (spring) features that change the load distributions in different ways as shown in Fig. 4(b). Thus, the composition of the force affects the performance of the modulator and some limitations are set by the pull-in effect of the actuator. To simplify the analysis later, the optical power is set to be a constant of 100 μW so the only variable quantity in the system is the actuation voltage. The modulator performance will be analysed in the pulse mode, sinusoidal mode and resonant mode. The 'one' and 'zero' state of each mode will be analysed as well.

3.1. Performance in the pulse mode

The performance of the modulator in the pull-in and initial states, with no electrostatic force applied, are investigated to figure out the maximum modifiable index range of the device. Here the pull-in state is regarded as the 'one' state and initial state is regarded as the 'zero' state. The pull-in voltage of the modulator in the pulse mode is shown in Fig. 5. From this plot, the allowed amount of voltage is dramatically decreased when the length of suspension (L) increased. This is the result of increased mass (M) and decreased stiffness (K) with a longer suspended section. This decreased stiffness indicates a smaller δ_{max} in the pull-in state with longer suspension length considering the equilibrium of the restoring force ($K \cdot x$), Casimir load and electromagnetic load. On the other hand, this decreased stiffness also indicates larger δ_{max} in the initial state with a longer suspended section as shown in Fig. 6(a). From Fig. 6(a), δ_{max} in the initial state and pull-in state intersect at a suspended length between 52 μm and 53 μm, which indicates the limits of the suspended length since the system collapse no matter what voltage is applied. In this case, modulation is impossible.

The corresponding effective index changes in the 'one' state and 'zero' state are shown in Fig. 6(b). The plot shows a larger value of Δn_{eff} with a longer suspended lengths in the initial state, when waveguide has Casimir and optical forces applied. It indicates that the load re-distribution on the waveguide is negligible with a short suspended length ($\leq$ 35 μm) due to the higher stiffness compared with longer suspended lengths. This non-linearly increasing index change with increasing suspended length degrades the modifiable effective index of the modulator with longer suspended lengths ($\geq 35 \mu m$). As the suspended length is increased, 35 μm is the point at

Optics EXPRESS

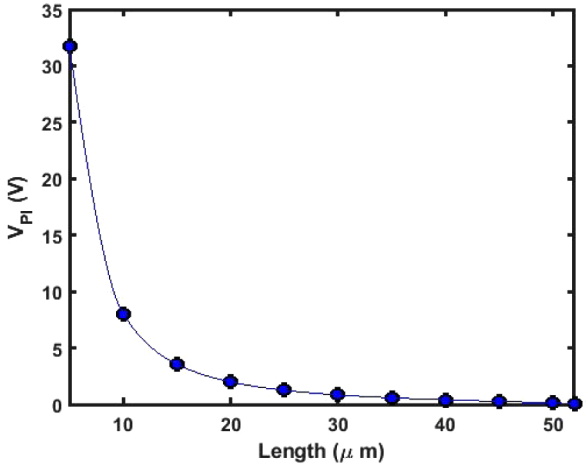

Fig. 5. Pull-in voltage (V_{PI}) of the modulator in the pulse mode with different suspended lengths

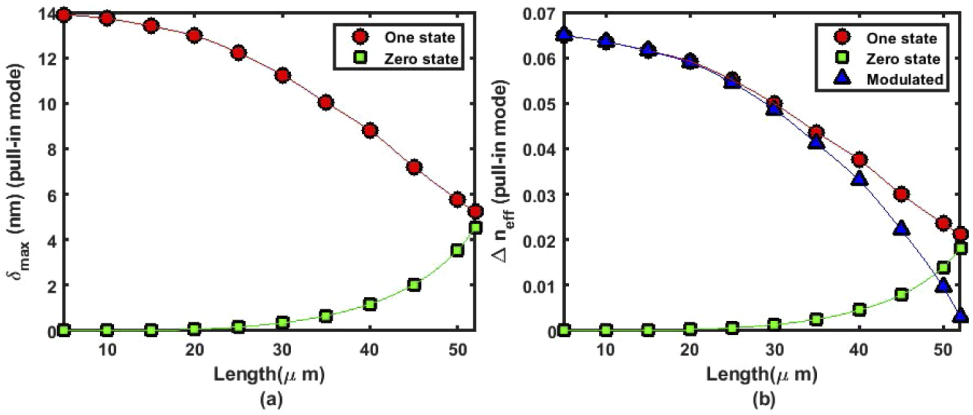

Fig. 6. (a) The maximum displacement (δ_{max}) on the deformation curves in the 'one' state and 'zero' state with different suspended lengths; (b) Effective refractive index change (Δn_{eff}) in the 'one' state and 'zero' state with different suspended lengths. The curve 'Modulated' is the is the index difference between the 'one' state and 'zero' state in the pulse mode, which is the maximum modifiable index change of the modulator. Both Figs. 6(a) and (b) are calculated by COMSOL Multiphysics

which the influence of Casimir and optical forces on the deformation curvature of the waveguide become comparable with the influence of the electrostatic force. Casimir and optical forces contribute to a large initial effective index change and degrade the tuning ability of the modulator for suspended lengths longer than 35 μm. As a consequence, the modifiable effective index change reaches a maximum about 0.065 with a length of 5 μm and almost 0 with a length of 52 μm in Fig. 6(b).The index changes shown in Fig. 6(b) are one order of magnitude higher than the typical values of index change shown in [11], which means the described suspended slot modulator consumes much less chip area compared with most active modulators.

The results of analytical approximations from Eq. (20), Eq. (21) and numerical solution from FEA software are shown in Fig. 7. The maximum effective index change and phase change of the device are 0.0649 (Fig. 7(a)) and 388.4° (Fig. 7(b)) with a suspended length of 5 μm and 30 μm,

Optics EXPRESS

respectively. It can be found that the analytical solution of the effective index and phase change are always larger than from FEA software as shown in Fig. 7, which means that the enhanced force applied on the structure deforms the waveguide in a different way to that in Eq. (13) and it contributes to a smaller index and phase change. The analytical approximation only shows a maximum difference of 7 % to 8 % in the pull-in state compared to result from the FEA software. This small error indicates that the load re-distribution caused by the force enhancement is not significant in the pulse mode. From Fig. 7, any suspended length between 12 μm and 47 μm can achieve a π shift in the normal state.

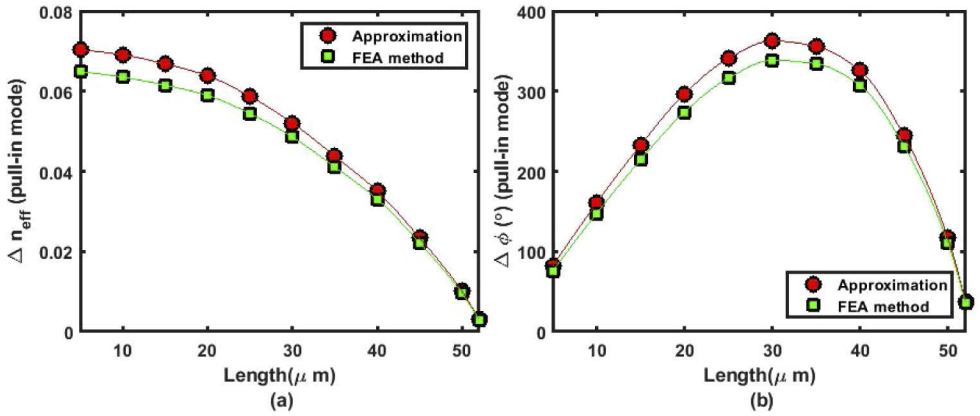

Fig. 7. The comparison of the index and phase changes ($\Delta n_{eff}, \Delta\phi$) between the theoretical approximation given by Eq. (20) Eq. (21) and the FEA method in the pulse mode with different suspended lengths; (a) The curve 'Approximation' is given by Eq. (20) and the curve 'FEA method' is the same as the curve 'Modulated' in Fig. 6(b); (b) The curve 'Approximation' is given by Eq. (21) and the curve 'FEA method' is calculated from the curve 'Modulated' in Fig. 6(b).

The forces applied in the system also affect the maximum allowable modulation frequency as shown in Fig. 8. Under the influence of both negative spring and air damping, the modulation frequency limit in the pull-in state is increased with increased length, while the frequency limit in the initial state experiences a ramp and drop with maximum at about 133 KHz. These two curves are the results of the product of decreased vibration frequency and increased air damping with increased length. The intersection of these two curves indicates that the frequency limitation (low) of described modulator is about 100 KHz. The actual operational frequency is in the region between the 'one' state and 'zero' state. According to Eq. (25), the modulation frequency can be further improved by increasing mechanical resonant frequency and air damping. A higher mechanical resonant frequency can be achieved by slot design with higher mechanical stiffness or by replacing the silicon with other materials with higher mechanical stiffness such as silicon nitride. Slot arms with larger width will increase mechanical resonant frequency while total index change and air damping are decreased. Higher air damping can be achieved by replacing air with other medium with higher viscosity such as water or having a longer suspending length according to Eq. (24). To allow for a longer suspended slot, a slot design with weaker optical force, weaker Casimir force, and stronger restoring force is required, which can be achieved by using different optical and electrical configurations.

3.2. Performance in the resonant mode

The modulator performance in the resonant mode is analysed using a sinusoidal drive since it presents the best modulator performance in the regime of sinusoidal mode. To make the

Optics EXPRESS

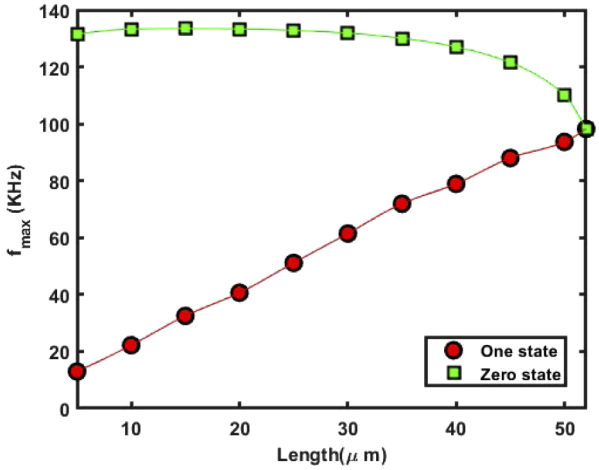

Fig. 8. The pulse modulation frequency limitation (f_{max}) at the initial ('zero') state and pull-in ('one') state with different suspended lengths

parameters in the sinusoidal mode comparable with the pulse mode, the maximum displacement on the deformation curvature in the 'one' state of the modulator in the sinusoidal mode is chosen to be the same as in 'one' state of the modulator in the pulse mode. With the same maximum displacement on the deformation curvature as in the pulse mode 'one' state, the actuating voltage of the modulator for all considered suspended lengths is significantly decreased in the resonant mode due to resonance based amplification. The equivalent actuating voltage amplitude from Eq. (30) in the 'one' state and the corresponding amplification factor for the different suspended lengths considered are shown in Fig. 9. From this plot, amplification factor of the modulator decreases with increasing suspended length. The amplification factors for the shorter lengths are extremely high due to decreased air damping according to Eq. (24) and Eq. (28). The maximum actuating voltage amplitude of the 'one' state is 2.45 V with a length of 5 μm. A typical value for the actuating voltage amplitude is 0.39 V with a length of 30 μm. The DC electrostatic, Casimir and optical forces apply a bias force on the suspended slot, which makes the beams deform differently in the 'one' state and the 'zero' state. The maximum displacement on the deformation curvature for the 'one' and 'zero' state and corresponding index changes are shown in Fig. 10. In the 'one' state of the resonant mode, maximum displacement of different suspended lengths is the same as with the 'one' state of the pulse mode. Negative values of the maximum displacement in the 'zero' state are calculated based on Eq. (31). The comparison of the modulated index and phase change between the theoretical approximation and FEA method for different lengths of the slot waveguide are shown in Fig. 11. In Fig. 11, the modulated index and phase changes solved by the FEA method are slightly increased compared with those in Fig. 7. The negative deformation curvature caused from repulsive electrostatic force in the 'zero' state contributes to the increased part of the modulated index and phase changes. The maximum effective index change and phase change of the device is 0.0828 (Fig. 11(a)) and 437.9° (Fig. 11(b)) with a suspended length of 5 μm and 35 μm, respectively. The numerical difference between the theoretical approximation and the FEA method is always less than 6 %. The resonant frequency of the suspended slot for different lengths as calculated using Eq. (27) is shown in Fig. 12. The resonant frequency of the modulator is much higher than the modulating frequency shown in Fig. 8. In the pulse mode, the modulating frequency is limited by τ to avoid distortion of the waveform (dispersion). While in the resonant mode, the modulator is excited with single frequency rather than a package of signals with different frequencies so the system settling time will not influence the modulating

Optics EXPRESS

frequency of the device. In Fig. 12, the highest resonant frequency is 84.6 MHz with a length of 5 μm. A typical value of resonant frequency is 2.33 MHz with a length of 30 μm. Even the smallest resonant frequency at 0.583 MHz with a length of 52 μm is almost 4.4 times larger than the maximum modulating frequency shown in Fig. 8.

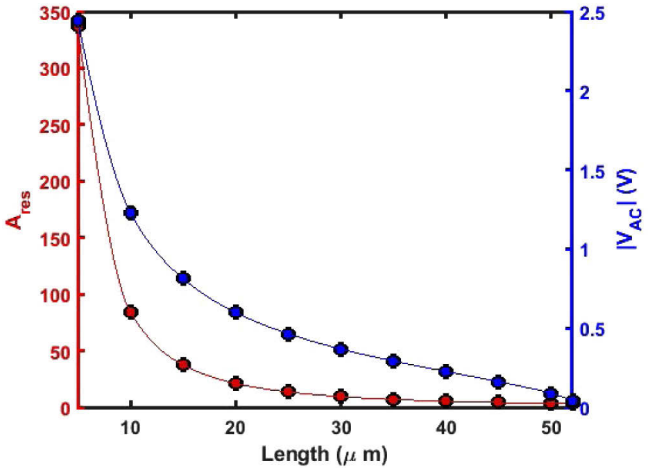

Fig. 9. Equivalent actuation voltage ($|V_{AC}|$) and force amplification factor (A_{res}) in the resonant mode with different suspended lengths.

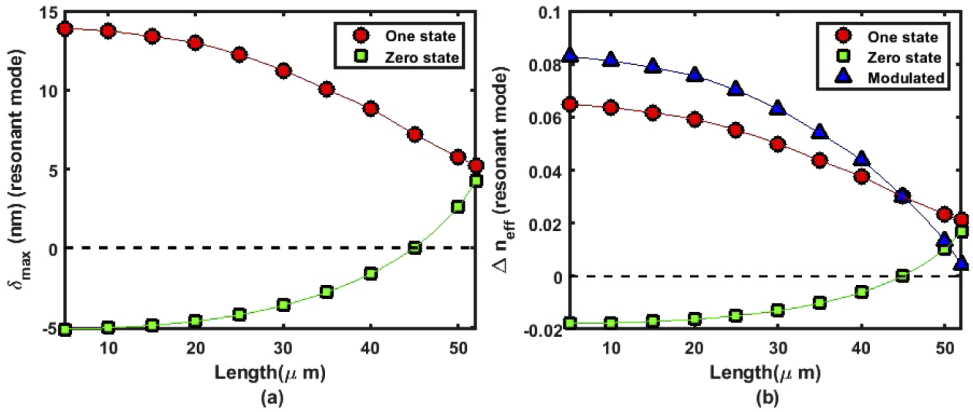

Fig. 10. (a) The maximum displacement (δ_{max}) on the deformation curves in the 'one' state and 'zero' state in the resonant mode with different suspended lengths; (b) Effective refractive index change (Δn_{eff}) in the 'one' state and 'zero' state with different suspended lengths. The curve 'Modulated' is the is the index difference between the 'one' state and 'zero' state in the resonant mode, which is the maximum modifiable index change of the modulator. Both Figs. 10(a) and (b) are calculated by COMSOL Multiphysics

3.3. Power consumption

The power consumption of the modulation evaluated by fJ/bit can be calculated by [23]:

$$E_{bit} = \frac{CV^2}{4} \tag{32}$$

Optics EXPRESS

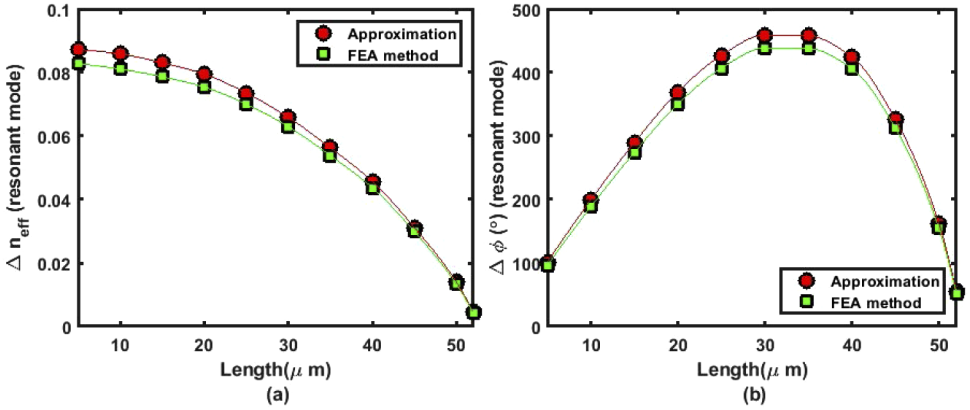

Fig. 11. The comparison of the index and phase changes ($\Delta n_{eff}, \Delta\phi$) between the theoretical approximation given by Eq. (20) Eq. (21) and the FEA method in the resonant mode with different suspended lengths; (a) The curve 'Approximation' is given by Eq. (20) and the curve 'FEA method' is the index difference between the 'one' state and 'zero' state of the modulator in the resonant mode by COMSOL Multiphysics; (b) The curve 'Approximation' is given by Eq. (21) and the curve 'FEA method' is calculated from the curve 'FEA method' in Fig. 11(a).

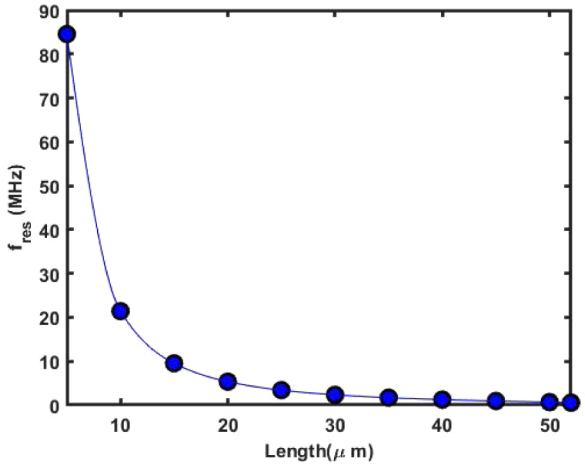

Fig. 12. Resonant frequency (f_{res}) of the modulator with different suspended lengths

One unique feature of the suspended slot modulator is that the capacitance will be changed by deformation of the slot arms so it closely relates to the actuation voltage and it is independent to the frequency of the square wave signal below f_{max}^{pulse}. The power consumption at the pull-in state of the pulse and resonant modes with the same modulation depth are shown in Fig. 13. In the pulse mode, the energy required per bit for is always less than 32 fJ/bit and decreases as the suspended length is increased. We can find an impressive value of 0.13 fJ/bit with a length of 30 μm. In the resonant mode, the energy required per bit is always less than 0.19 fJ/bit. The energy consumption with a length of 30 μm is further decreased to 0.025 fJ/bit. The energy consumption in the resonant mode is even less than that in the pulse mode for all lengths, reaching levels that are unachievable using most other active modulators such as described in

Optics EXPRESS

[11], [24], and [25]. Moreover, there is no optical absorption contributing to excess loss during the modulation as with plasma dispersion based approaches.

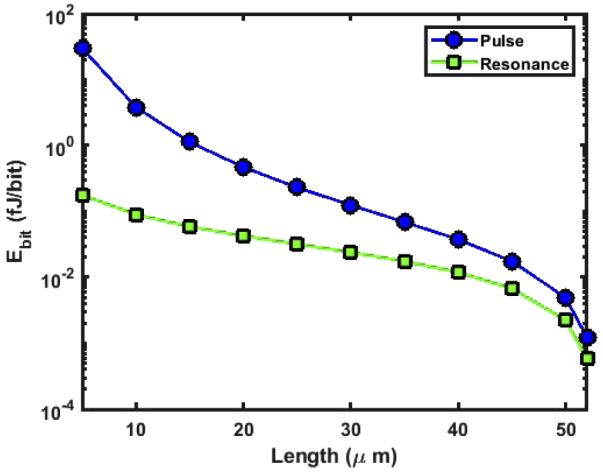

Fig. 13. The energy cost of the modulation (E_{bit}) in the pulse and resonant mode with different suspended lengths.

3.4. Modulator construction

The modulator can be constructed by cascading multiple suspended slot waveguide segments into a mach-zhender interfrometer (MZI) or a ring resonator modulator. Multiple identical segments can effectively decrease the actuating voltage with a given value of total effective index change and phase change, thus a lower power consumption can be achieved. Furthermore the active modulator can be constructed with each segments having a different suspended lengths providing more flexibility in the design. Fortunately, the length of a single segment of suspended slot will not exceed 52 μm based on the calculations above so the size of the modulator is easily controlled. This opto-mechanical modulation not induce additional light absorption in the C-band so the propagating loss during modulation is extremely low. The most significant cause of loss is likely to result from the mode conversion between suspended and supported slot waveguides.

As proven by the simulation results, the best modulator performance is obtained by operating in the resonant mode at mechanical resonant frequency. Power dependent optical forces can significantly influence the system with a high power input (mW level) as measured in [10] or field enhancement [26]. For a specific mode shape with a specific suspended length of suspended slot, mechanical resonance provides very narrow modulating bandwidth. To expand modulating bandwidth, non-identical suspended lengths on different segments must be considered. The mechanical resonant frequency of each segment can be tuned by using an offset voltage or different input optical power to adjust modulating bandwidth. A higher modulating frequency in the resonant mode can be achieved by exciting mechanical resonance at higher frequencyies. However, the mode shape (deformation curvature) of higher order mechanical resonant modes must degrade the index and phase change of the modulation. In this case, a trade-off between the modulating frequency and modulation depth is required.

The geometrical parameters defining on the cross-section of the suspended slot can be adjusted to optimise the performance depending on the specific requirements. The larger the separation between the slot arms the lower the Casimir and optical forces and therfore the critical displacement of the slot arms is enlarged allowing for a better modulation depth to be expected. A thicker slot waveguide can generate a larger optical force, Casimir force and electrostatic force

Optics EXPRESS

so less energy is required in actuation. A wider slot waveguide changes the magnitude of the optical force and effective index dependence on the separation between slots arms. Moreover, the mechanical resonant frequency is increased with higher mechanical stiffness as measured in [3]. In this case, a higher modulating frequency is obtained along with a higher modulation depth in the pull-in state with higher power consumption in modulation. As a result, any geometrical changes will affect the performance of the modulator. Generally, the overall performance of the modulator will be in a region between a carrier-based approach and MOEMS approach and could serve a number of niche application for which its performance is well suited.

4. Conclusions

In this paper, the performance of a silicon NOEMS electro-optic modulator based on a slot waveguide is analysed (t=220 nm, w=280 nm, g=70 nm) involving Casimir, optical and electrostatic forces for the fundamental quasi-TE mode. Single segments of the suspended slot waveguide are evaluated for suspended lengths from 5 μm to 52 μm. Caisimir and optical forces significantly influence the system limitations for longer suspended lengths. Simulation results show that the maximum suspended length is around 52 μm. In the pulse mode, the maximum effective index change and phase change of the device are 0.0649 and 388.4° with a suspended length of 5 μm and 30 μm, respectively. The maximum actuating voltage is 31.7 V with a suspended length of 5 μm. The highest modulating frequency of the modulator is 120 KHz with a suspended length of 15 μm considering the influence of air damping. In the resonant mode, the maximum effective index change and phase change of the device is 0.0828 and 437.9° with a suspended length of 5 μm and 35 μm, respectively. The maximum actuating voltage is 2.44 V with a suspended length of 5 μm. The highest modulating frequency of the modulator is 84.6 MHz with a suspended length of 5 μm. The power consumption of the modulation can be low as 0.13 fJ/bit and 0.025 fJ/bit in the pulse and resonant modes, respectively. These results indicate that a waveguide with a length in the range of 20 μm to 35 μm has the best comprehensive performance. Simulation results prove that the suspended slot modulator has the advantages of low actuation voltage and power consumption, large effective index and phase change compared with other active modulator approaches.

A MZI-based modulator or a ring resonator based modulator can be constructed from the suspended slot waveguide. A low actuating voltage and power consumption can be expected when the modulator is constructed by cascading multiple suspended slot waveguide segments. Integrating segments of suspended slot with different suspended lengths provides more flexibility in design. The most significant cause of optical loss is likely to result from mode conversion between the suspended and supported slot waveguides. The geometrical parameters on the cross-section of the suspended slot can be adjusted to optimise the performance to meet specific requirements. The performance of such a modulator can fill the performance gap between carrier-based and MOEMS based modulators.

Funding

Engineering and Physical Sciences Research Council (EP/V000624/1).

Acknowledgments

The authors thank silicon photonics group for necessary guidance and assistance in the simulations. Yu Feng acknowledges scholarship from the China Scholarship Council for his PhD study. Dr. David J. Thomson acknowledges funding from the Royal Society for his University Research Fellowship.

Optics EXPRESS

Disclosures

The authors declare no conflicts of interest.

References

1. V. R. Almeida, Q. Xu, C. A. Barrios, and M. Lipson, "Guiding and confining light in void nanostructure," Opt. Lett. **29**(11), 1209–1211 (2004).
2. M. Li, W. Pernice, C. Xiong, T. Baehr-Jones, M. Hochberg, and H. Tang, "Harnessing optical forces in integrated photonic circuits," Nature **456**(7221), 480–484 (2008).
3. J. Roels, I. De Vlaminck, L. Lagae, B. Maes, D. Van Thourhout, and R. Baets, "Tunable optical forces between nanophotonic waveguides," Nat. Nanotechnol. **4**(8), 510–513 (2009).
4. E. M. Lifshitz and M. Hamermesh, "The theory of molecular attractive forces between solids," in *Perspectives in Theoretical Physics*, (Elsevier, 1992), pp. 329–349.
5. V. R. Almeida and R. R. Panepucci, "Nano-opto-electro-mechanical devices based on silicon slot-waveguides structures," in *2009 SBMO/IEEE MTT-S International Microwave and Optoelectronics Conference (IMOC)*, (IEEE, 2009), pp. 560–563.
6. K. Van Acoleyen, J. Roels, P. Mechet, T. Claes, D. Van Thourhout, and R. Baets, "Ultracompact phase modulator based on a cascade of NEMS-operated slot waveguides fabricated in silicon-on-insulator," IEEE Photonics J. **4**(3), 779–788 (2012).
7. J. R. Rodrigues, F. S. S. Rosa, and V. R. Almeida, "Casimir and optical forces acting on a silicon noems device based on slot-waveguide structure," IEEE Photonics Technol. Lett. **28**(5), 589–592 (2016).
8. F. De Leonardis, M. De Carlo, and V. Passaro, "Design rules for a nano-opto-mechanical actuator based on suspended slot waveguides," Photonics **4**(4), 43 (2017).
9. D. Thomson, A. Zilkie, J. E. Bowers, T. Komljenovic, G. T. Reed, L. Vivien, D. Marris-Morini, E. Cassan, L. Virot, J.-M. Fédéli, J.-M. Hartmann, J. H. Schmid, D.-X. Xu, F. Boeuf, P. OBrien, G. Z. Mashanovich, and M. Nedeljkovic, "Roadmap on silicon photonics," J. Opt. **18**(7), 073003 (2016).
10. K. Y. Fong, W. H. Pernice, M. Li, and H. X. Tang, "Tunable optical coupler controlled by optical gradient forces," Opt. Express **19**(16), 15098–15108 (2011).
11. G. T. Reed, G. Mashanovich, F. Y. Gardes, and D. Thomson, "Silicon optical modulators," Nat. Photonics **4**(8), 518–526 (2010).
12. W.-C. Chiu, C.-C. Chang, J.-M. Wu, M.-C. M. Lee, and J.-M. Shieh, "Optical phase modulators using deformable waveguides actuated by micro-electro-mechanical systems," Opt. Lett. **36**(7), 1089–1091 (2011).
13. M. L. Povinelli, M. Lončar, M. Ibanescu, E. J. Smythe, S. G. Johnson, F. Capasso, and J. D. Joannopoulos, "Evanescent-wave bonding between optical waveguides," Opt. Lett. **30**(22), 3042–3044 (2005).
14. P. T. Rakich, P. Davids, and Z. Wang, "Tailoring optical forces in waveguides through radiation pressure and electrostrictive forces," Opt. Express **18**(14), 14439–14453 (2010).
15. F. Beer, E. Johnston, and J. DeWolf, "Mechanics of materials, 5th si edition," Stress **1**, 1–12 (1999).
16. J. M. Amiss, F. D. Jones, and H. H. Ryffel, *Guide to the Use of Tables and Formulas in Machinery's Handbook* (Industrial Press Inc., 2004).
17. S. Pamidighantam, R. Puers, K. Baert, and H. A. Tilmans, "Pull-in voltage analysis of electrostatically actuated beam structures with fixed–fixed and fixed–free end conditions," J. Micromech. Microeng. **12**(4), 319458 (2002).
18. H. C. Nathanson, W. E. Newell, R. A. Wickstrom, and J. R. Davis, "The resonant gate transistor," IEEE Trans. Electron Devices **14**(3), 117–133 (1967).
19. Y. Sun, D. Fang, and A. K. Soh, "Thermoelastic damping in micro-beam resonators," Int. J. Solids Struct. **43**(10), 3213–3229 (2006).
20. C. Zhang, G. Xu, and Q. Jiang, "Analysis of the air-damping effect on a micromachined beam resonator," Math. Mech. Solids **8**(3), 315–325 (2003).
21. Z. Hao, A. Erbil, and F. Ayazi, "An analytical model for support loss in micromachined beam resonators with in-plane flexural vibrations," Sens. Actuators, A **109**(1-2), 156–164 (2003).
22. G. K. Fedder, C. Hierold, J. G. Korvink, and O. Tabata, *Resonant MEMS: fundamentals, implementation, and application*, vol. 22 (John Wiley & Sons, 2015).
23. D. A. Miller, "Energy consumption in optical modulators for interconnects," Opt. Express **20**(S2), A293–A308 (2012).
24. C. Xiong, D. M. Gill, J. E. Proesel, J. S. Orcutt, W. Haensch, and W. M. Green, "Monolithic 56 gb/s silicon photonic pulse-amplitude modulation transmitter," Optica **3**(10), 1060–1065 (2016).
25. J. Witzens, "High-speed silicon photonics modulators," Proc. IEEE **106**(12), 2158–2182 (2018).
26. D. Van Thourhout and J. Roels, "Optomechanical device actuation through the optical gradient force," Nat. Photonics **4**(4), 211–217 (2010).